Leveraging U-NET to map Brazilian Atlantic Forest's Active Restoration using Remote Sensing data.

Felipe Nincao Begliomini

Advisor: Dr. D. Coomes
Dr. C. Wheeler
Dr. S. Keshav

AI4ER CDT
University of Cambridge

A Thesis submitted for the Degree of
Master of Research in Environmental Data Science
In the Dept. of Earth Sciences

June 2023

This report is the result of my own work and includes nothing which is the outcome of work done in collaboration, except where specifically indicated in the text and/or bibliography.

Word Count: 4979

Table of Contents

Abstract

The Atlantic Forest, a globally significant biodiversity hotspot, has suffered severe degradation and deforestation, prompting increased attention towards ecological restoration initiatives. Active restoration, a widely employed strategy in the Atlantic Forest, involves human interventions to accelerate ecosystem recovery. However, monitoring active restoration sites is hindered by the lack of a centralized database, limiting the information needed for effective public policies to restore the biome. To address this challenge, we aim to lower the barriers to creating and maintaining an accurate, central database of restoration efforts. Our approach relies on the automatic detection of active restoration areas using Machine Learning on high-resolution (5m) optical- and RADAR remote sensing imagery. We utilized a comprehensive (~213 km^2) ground truth dataset of active restoration sites in the Atlantic Forest for calibrating and testing our models. It was split into two sets for distinct experiments, including all polygons and a higher-quality polygons subset. Using the U-NET architecture, a widespread model for image segmentation, we evaluated optical spectral- and temporal metrics to perform the classification. Additionally, we proposed an innovative U-NET configuration for integrating multi-resolution RADAR and optical data. Our results revealed that the experiment utilizing spectral data alone in the subset data yielded the best overall results (Dice Score=0.4), likely influenced by polygon quality and landscape homogeneity. We hypothesize that the underperformance of temporal metrics among all tested models in both experiments could be due to potential georeferencing errors in the image. However, the experiment analyzing the complete dataset demonstrated that integrating different remote sensing data modalities outperformed other models, improving discrimination in complex landscapes. To increase the models' accuracy, we suggest enhancing the quality of the ground truth dataset and exploring different hyperparameter configurations. Our findings demonstrate the potential of remote sensing-based methodologies for monitoring active restoration in the Atlantic Forest, which could provide valuable insights for environmental restoration policies.

Keywords: Remote Sensing, Active Restoration, Atlantic Forest, Deep Learning.

1 Introduction

The climate and biodiversity crisis has spotlighted Brazil as a priority region for global conservation efforts. The Amazon Forest has attracted significant international resources to curb deforestation, but less attention has been paid to protecting other biomes in the country. Due to intense resource exploitation dating back to the Portuguese colonization, the once-vast Atlantic Forest was reduced to less than a fifth of its original extent [1]. However, even though its area is only about 3% of the Amazon basin, this endangered biome contributes disproportionally to the biodiversity in South America. The Atlantic Forest is home to over 20,000 plant species and contains the largest number of Brazilian endemic and small-ranged vertebrates [2]. Considering its high biodiversity value and imminent threat, the Atlantic Forest is recognized as a globally significant biodiversity hotspot that should be prioritized for conservation [3].

Deforestation prevention plays an important role in preserving the remaining Atlantic Forest. The biome was the first in Brazil to have specific regulations against deforestation, which has legally protected all the remaining primary forest fragments (i.e., without significant human disturbance) since 2006 [4]. But even with these strict laws, long-term monitoring still identifies alarming deforestation rates. For instance, 210 km^2 were lost between 2020 and 2021 out of the ~162,000 km^2 of remaining forest [5]. While efforts to prevent deforestation are crucial, it has become evident that halting deforestation alone is not sufficient to rebuild the biome's integrity and restore its vital ecosystem services. This realization has shifted focus towards Atlantic Forest's ecological restoration as a national priority. As a result, the United Nations (UN) recognized the efforts made by Brazil, Paraguay, and Argentina to restore the Atlantic Forest as one of the 10 World Restoration Flagships for the UN Decade on Ecosystem Restoration [6]. This award was given to the "most ambitious, visionary, and promising ecosystem restoration initiatives" acknowledged by the UN.

Ecological or Ecosystem Restoration is "the assisted process of returning a degraded, damaged, or destroyed ecosystem to a previous state close to its natural condition" [7]. Ecological Restoration initiatives can be divided into two broad classes. Passive Restoration (PR) is the strategy where human inputs are restricted to only a few actions to remove environmental stressors (e.g., grazing), giving the necessary conditions for the

forest to restore itself [8]. In contrast, Active Restoration (AR) applies various techniques to enhance the regeneration of the degraded landscape [9]. The deployed strategy is usually chosen considering the level of landscape degradation, expected time to recover, and budget constraints. PR requires considerably less investment and human labor, but achieving satisfactory restoration rates in degraded ecosystems is expected to take decades [10]. On the other hand, AR can be applied to restore environments in any stage of degradation with a relatively predictable restoration trajectory but at a high financial cost [11]. In the context of Atlantic Forest restoration, specialists are more likely to choose AR considering the severely degraded nature of many landscapes and long distances from native fragments that provide the seed sources for natural regrowth [12].

Improving the monitoring of secondary forests, whether from PR or AR, is important for informing public policies and developing better strategies to rebuild endangered biomes and mitigate climate change [13]. Fortunately, there has been a significant increase in the implementation of AR initiatives in the Atlantic Forest in recent years [14], and it is vital to keep track of these projects to ensure successful biome restoration [15]. However, creating a centralized database for Atlantic Forest AR areas is challenging due to the various motivations, stakeholders, and administrative levels involved. To overcome these challenges, Satellite Remote Sensing (SRS) has emerged as a valuable tool for obtaining scalable and timely information on recovering landscapes [16]. While Brazil has a long-standing SRS-based program for monitoring tropical forests, the spatial resolution (30 m) often falls short in precisely monitoring ecological restoration sites [17,18]. Therefore, considering the limited spatial and temporal granularity of current efforts to track AR sites, there is a pressing need for new methodologies to inform environmental policies [19].

Therefore, this study aimed to lower the barriers to creating a centralized AR database by deploying an automatic detection methodology using Machine Learning on high-resolution optical imagery. We utilized the most comprehensive dataset of AR polygons in the Atlantic Forest, evaluating the effectiveness of the widely used U-NET architecture in three configurations and two subsets of the available ground-truth dataset. Additionally, RADAR imagery was incorporated to enhance the identification of AR. This study's key contributions include the first large-scale and high-resolution (5 m) attempt to map

regrowing forests using a specific ecological restoration strategy and proposing an innovative framework for fusing different SRS modalities with the U-NET architecture.

2 Research Questions

This study aims to investigate the following research questions:

- Q1: To what extent can sites of active forest restoration be mapped using satellite remote sensing imagery?

- Q2: To what extent do temporal remote sensing metrics produce higher classification accuracy than spectral metrics from a single time epoch?

- Q3: To what extent does fusing different remote sensing modalities increase the accuracy of the predictions?

3 Materials and Methods

This section provides a detailed description of the methodology used in the study. First, we presented the study area and the ground truth dataset of AR polygons. We outlined filtering procedures and the selection of two specific Regions of Interest (ROI) for conducting two separate experiments. Next, we described the SRS datasets and the process of generating image chips to be used as input for the U-NET architecture. Subsequently, we introduced the three U-NET configurations and the evaluation metrics. The SRS images in the study were consumed and pre-processed using the Google Earth Engine platform (GEE). The U-NET models were developed on the Massive GPU Cluster for Earth Observation (MAGEO) provided by the NERC Earth Observation Data Acquisition and Analysis Service.

3.1 Study Area

This study focuses on the Southeast and Southern regions of the Atlantic Forest, which encompass three distinct forest types: Dense Rain Forest, Mixed Rain Forest, and Seasonal Forests [20]. These regions experience a range of climatic conditions, with mean annual temperatures varying from 11°C to 26°C and mean annual rainfall ranging from 700 mm to 3120 mm [21]. For our analysis, we have identified two specific areas of interest here defined as Region of Interest 1 (ROI 1) and Region of Interest 2 (ROI 2) (Figure 1). Detailed descriptions of these regions are provided in the following sections.

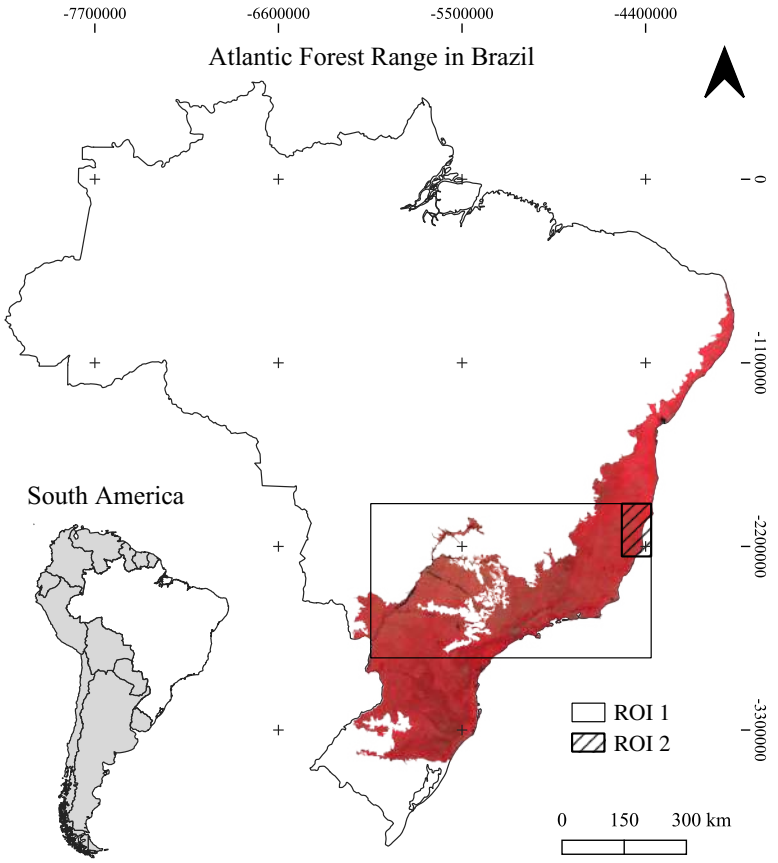

Figure 1. The Brazilian Atlantic Forest is highlighted in the false-color composition. The hatched and black contour polygons delimit the Regions of Interest (ROI).

3.1.1 Active Restoration polygons dataset

We used a comprehensive dataset of AR polygons for the Atlantic Forest, provided by a consortium of Brazilian partners from academia, private companies, state entities, and NGOs. Unfortunately, **we cannot share the database or provide specific location details** due to data access restrictions and sensitive information. Nevertheless, we processed the dataset using the following steps.

3.1.2 Dataset pre-processing

The dataset provided by each partner included geofiles in various formats and contained metadata information at multiple levels. It comprised polygons representing different restoration techniques, including areas without implemented ecological restoration. Several filtering steps were performed to create a focused and representative set of AR initiatives (Table 1). First, only polygons labeled as 'Active Restoration' were selected. Then, polygons with precise planting years and labeled as either 'In restoration' or 'Restored' were retained. The analysis considered initiatives planted until 2019, aligning with the available SRS data. Additionally, polygons with a total area of less than 0.01 km^2 were filtered out to match the spatial resolution constraint of the available high-resolution SRS data (5 m). The last described step removed 3,704 polygons, representing around 0.01% of the total area. Finally, a spatial filter was applied to ensure that all polygons fell within the boundaries of the Atlantic Forest.

Table 1. Filters applied to the Active Restoration polygons dataset.

Filters	Criteria
Method	Active Restoration
Year	<= 2019 and Not Null
Area	> 0.01 km^2
Limits	Inside Atlantic Forest

All data sources were reprojected to the same coordinate reference system (WGS 84 / Pseudo-Mercator) and visually inspected for misalignment after the conversion. Finally, the layers were compiled into a single GeoPackage file. The resulting dataset comprised

9,556 polygons, representing a total area of ~213 km^2 of AR sites within the Atlantic Forest. The compiled polygons file was converted from the vector to the raster format in a resolution of 5 meters and uploaded to GEE to make it adequate for U-NET classification masks. It is worth noting that the filtering procedure required a substantial amount of time during the project period, spanning approximately one month. This extended duration was necessary due to the complexity and initial state of the dataset.

3.1.3 Delimitating the Regions of Interest

Exploratory data analysis showed that the data providers had varying quality levels of metadata information associated with each polygon. Additionally, the criteria used to define the ecological restoration area showed inconsistencies, such as incorporating fragments of native forest in the intervention polygon (Figures 2C and 2F). We also observed geographical misplacements unrelated to reprojection (Figures 2B and 2E). Furthermore, certain regions exhibited no significant changes in land use or evidence of forest regrowth, despite almost a decade of SRS observations (Figures 2A and 2D). Due to our study's time limitations, we could not invest in enhancing and refining the polygons to obtain a higher-quality dataset. However, we found that the dataset's most reliable source contained a region with a high density of ecological restoration sites not overlapped by polygons from other layers. As a result, we conducted a separate experiment within this region to evaluate the extent to which the dataset's quality could influence the outputs of our model. It is worth noting that this reduced area region possesses a more homogeneous land cover and land use than the larger dataset, which encompasses many polygons in the complex landscape of São Paulo State. Therefore, we designated the entire available dataset as ROI 1, while ROI 2 represents the reduced region with a less intricate landscape. ROI 2 consists of 4,537 polygons covering an area of ~111 km^2 (Figure 1).

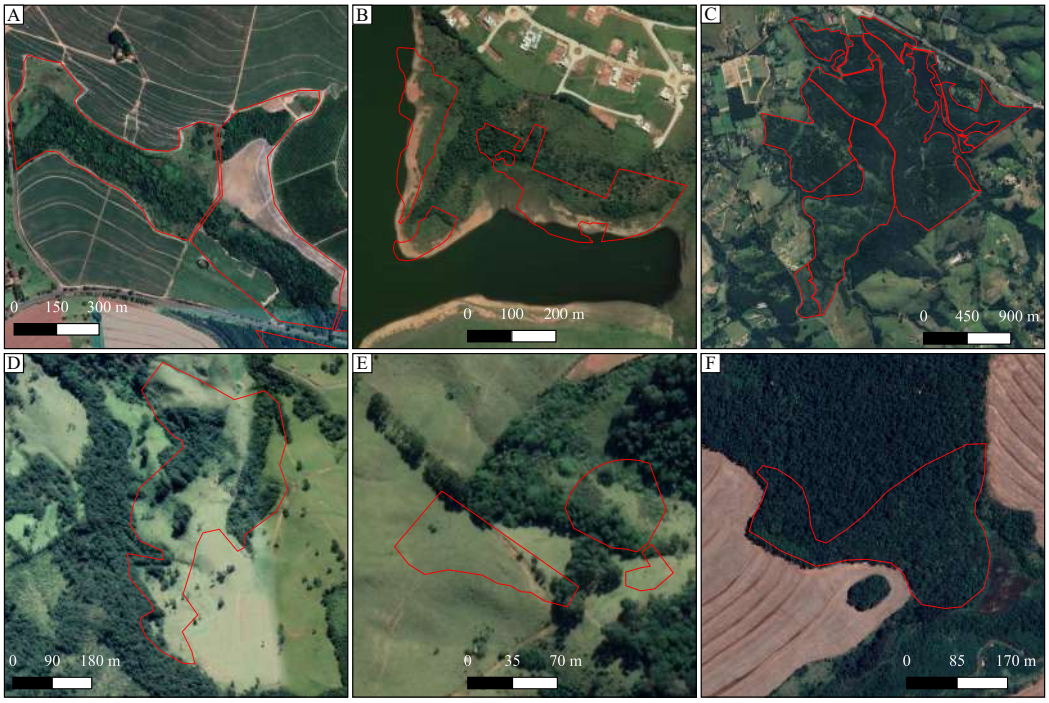

Figure 2. Examples illustrating limitations in the ground truth dataset. Satellite images sourced from Google Earth. A and D show regions without observable land use change. B and E demonstrate misaligned polygons. C and F depict polygons encompassing native or advanced secondary forests within the active restoration polygons.

3.2 Satellite Remote Sensing Datasets

This section details the SRS layers used in the study and the pre-processing techniques employed. Appendix C provides a comprehensive overview of AR remote sensing and explains the rationale behind selecting the presented layers for the analysis.

- Planet Scope: Derived from the Norwegian government's International Climate and Forests Initiative Satellite Data Program, it is the largest SRS high-resolution optical freely available dataset for tropical regions. Planet Scope provides high-resolution optical imagery in basemaps temporal composites (6-months or 1-month) at approximately 5 meters resolution, featuring four spectral bands (Blue, Green, Red, and Near-Infrared). Spanning from 2015 to 2023, this data offers an extensive, nearly decade-long record of high-resolution landscape changes.

- Sentinel-1: As part of the European Space Agency's Copernicus program, Sentinel-1 is a SAR satellite operating in C-Band since 2014. The mission was composed of two satellites, Sentinel-1A and Sentinel-1B. However, in December 2021, Sentinel-1B experienced a technical failure and was decommissioned. This resulted in a temporary loss of coverage in certain regions until the launch of Sentinel-1C, expected for the next few years. The best-resolution available product is at 10 meters in Single co-polarization VV (Vertical transmitted / Vertical received) and Dual-band cross-polarization VH (Vertical transmit/Horizontal receive) with a temporal resolution of 12 days.

- ALOS/PALSAR-2: Inherited from one of the oldest programs of L-Band SAR satellites, the Japanese Earth Resources Satellite (JERS), ALOS/PALSAR-2 has been effectively capturing global imagery since 2014. Initially, the data was not readily accessible, but the Japan Aerospace Exploration Agency recently made yearly composites available for public use. These composites are provided at a resolution of 25 meters in Single co-polarization HH and Dual-band cross-polarization HV from 2014 to 2020.

To ensure consistency in our analysis, 2020 was established as the temporal reference point due to the unavailability of certain selected layers beyond that year. The initial pre-processing step involved creating median yearly composites for Planet Scope and Sentinel-1 data, specifically for 2016, 2018, and 2020. ALOS/PALSAR-2 dataset was filtered to include layers only from the same years. Subsequently, we calculated the NDVI using Planet's Near-Infrared and Red bands (Near-Infrared - Red / Near-Infrared + Red) [22]. Lastly, all images were reprojected to the same coordinate reference system (WGS 84 / Pseudo-Mercator) to align the gridding and maintain spatial coherence throughout the analysis. A nearest-neighbor policy was employed during the reprojection to avoid potential discrepancies from the original data.

3.3 Image Chips Generation

Generating image chips in a compatible format with U-NET posed significant challenges during the development of this study. While the image processing itself was straightforward within the GEE platform, the integration of the cloud database and Machine Learning development environments remains poorly developed. Additionally, GEE's limitations in downloading large imagery hindered the transfer of complete pre-processed layers. To address these issues, we designed a pipeline that allows for the downloading smaller image patches, facilitating their manipulation and ingestion into U-NET. Our pipeline takes a point geometry as input and generates a square buffer with a side length of 3 kilometers, ensuring efficient and manageable downloads. Figure 3 illustrates the strategy to maximize the number of generated image chips considering the AR polygons dataset. The first step involved taking the filtered polygons and creating a regular grid of 2 km^2. Subsequently, only the cells that intersected with the polygons were chosen. Finally, the centroid of each selected cell was extracted and utilized as input for downloading the image chips.

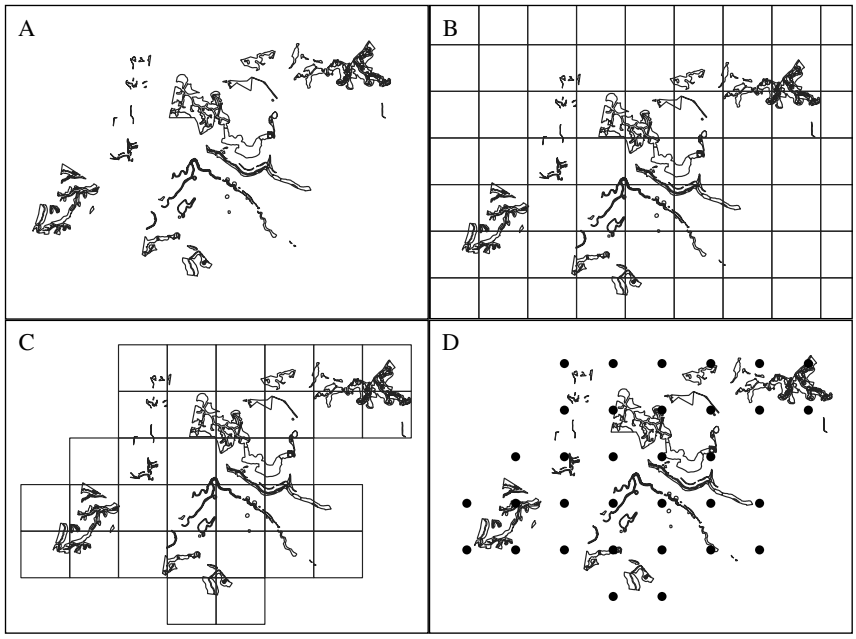

Figure 3. Sampling strategy for generating image chips. A) Sample of the filtered polygons dataset. B) Regular grid (2 km^2) over the sampling region. C) Cells selected with polygon intersections. D) Points generated from cell centroids.

For each sampling point, a total of five images were downloaded to MAGEO:

- Reference image (1 band): Binary mask obtained after rasterizing the polygon dataset (Section 5.2.1) in a resolution of 5 meters.
- Planet image (4 bands): Blue, green, red, and near-infrared bands from the 2020 temporal composite in a resolution of 5 meters.
- Planet NDVI (3 bands): NDVI yearly composites from 2016, 2018, and 2020 in a resolution of 5 meters
- Sentinel-1 (3 bands): C-Band VH polarization yearly composites from 2016, 2018, and 2020 in a resolution of 10 meters.
- ALOS/PALSAR-2: L-Band HV polarization yearly composites from 2016, 2018, and 2020. Although the original resolution of the dataset is 25 meters, it was upsampled to 20 meters to be compatible with the designed U-NET architecture. The nearest-neighbor policy was chosen to minimize data degradation.

Choosing the appropriate spatial extent to be represented by the image chips plays a crucial role in enhancing the effectiveness of semantic segmentation [23]. Aguiar [24] observed a relationship between restoration initiatives and certain landscape features, where AR in the Atlantic Forest tended to be near rivers, native forest fragments, and flat terrains. Therefore, we set the image chips to represent an area of 2 km^2, encompassing a portion of the surrounding landscape to potentially include elements that aid in identifying the AR initiatives. We added a 1-kilometer security margin to the buffer used for downloading the images to ensure the inclusion of the desired area. After downloading, we cropped the image chips to the same spatial resolution. The reference raster and Planet Scope-derived images were cut to a resolution of 400x400 pixels, while the Sentinel-1 and ALOS/PALSAR-2 images were reduced to 200x200 and 100x100 pixels, respectively. We normalized each image, scaling the values between 0 and 1 based on the designed value range for each layer. Planet Scope images were divided by 10000, NDVI images were normalized to a range of -1 to 1, Sentinel-1 imagery was normalized between -50 and 1, and ALOS/PALSAR-2 imagery was divided by 10000. Figure 4 shows an example of the SRS image chips with the reference mask highlighted in red.

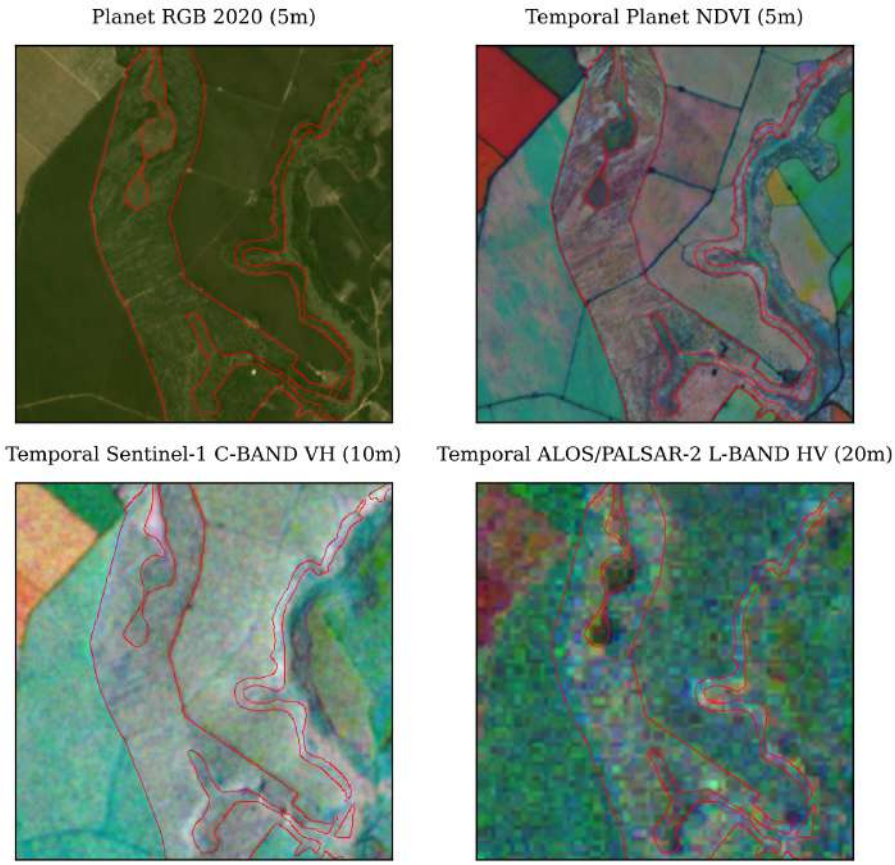

Figure 4. Example of the Satellite Remote Sensing image chips with the reference mask highlighted in red.

3.4 U-NET

The final step in the methodology was running the U-NET models with the generated image chips. Appendix D provides additional details regarding the U-NET architecture and its previous applications in forestry remote sensing. We propose three configurations based on the original architecture: U-NET RGBN, U-NET NDVI, and U-NET Fusion (Figure 5). Each one differs in the SRS layers used as input data. In U-NET RGBN, the 4-band Planet image 2020 yearly composite is utilized as input, along with the reference masks. U-NET NDVI employs the Planet NDVI temporal 3-bands to generate the corresponding reference. The U-NET Fusion configuration introduces a novel modification to the U-NET structure, allowing for the inclusion of different SRS layers with varying spatial resolutions. In the top level, the same Planet NDVI image is inputted, and after reducing its spatial resolution by half using the Max Pooling operation, the Sentinel-1 image is concatenated at the second level. The same procedure is repeated with the ALOS/PALSAR-2 image at the third level.

The implemented U-NET models followed the standard depth of 5 levels and the number of filters specified in by Ronneberger et al. [25]. Down-sampling layers consisted of two convolutions, batch normalization, ReLU activation, and max pooling with stride 1 and padding 1 to maintain the input size. Up-sampling layers employed transposed convolutions and concatenated skip connections. The final segmentation output used a 1x1 convolution followed by sigmoid activation. The training utilized a learning rate of 1e-4, a batch size of 16, and 100 training epochs. The loss function employed during training was the dice loss due to its suitability for handling unbalanced datasets [26]. We used augmentation to double the number of images in the training. Augmentation included random rotation (35 degrees limit), horizontal flipping (50% probability), and vertical flipping (10% probability). We trained the 3 U-NET configurations in two different experiments. Experiment 1 had 2612 image chips from ROI 1, while Experiment 2 had 751 from ROI 2. The data was split into 80% training and 20% testing. After training, the following accuracy metrics were computed by aggregating the outputs of all individual models:

$$Overall\ Accuracy = \frac{True\ Positive}{Positive + Negatives}$$

$$Dice\ Score = \frac{(2\ *\ True\ Positive)}{(2\ *\ True\ Positive\ +\ False\ Positive\ +\ False\ Negative)}$$

$$Precision = \frac{True\ Positive}{True\ Positive + False\ Positives}$$

$$Recall = \frac{True\ Positive}{True\ Positive\ +\ False\ Negatives}$$

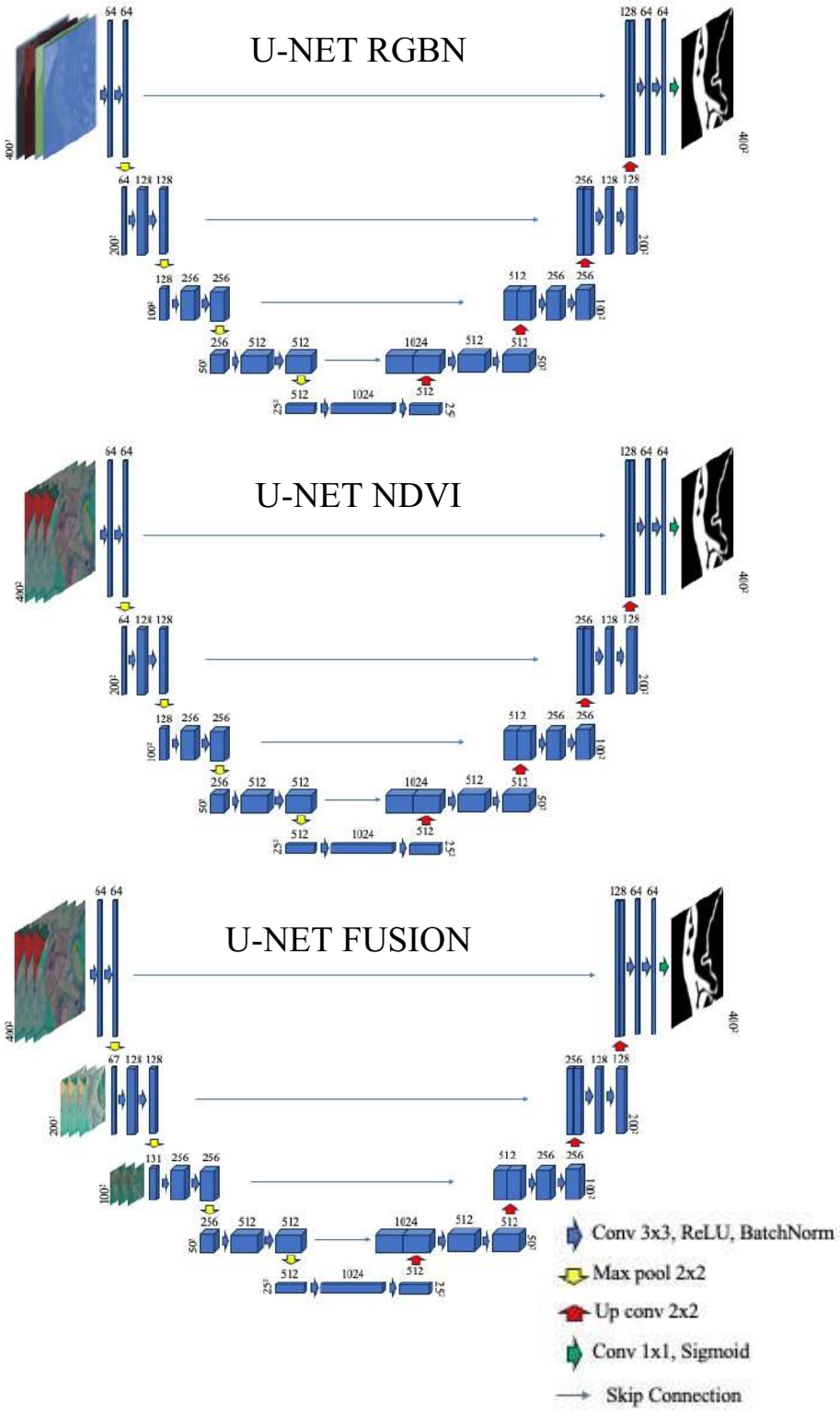

Figure 5. Three U-NET model configurations: U-NET RGBN, U-NET NDVI, and U-NET Fusion. These configurations employ different SRS layers as input data, enabling effective image analysis and classification.

4 Results

4.1 Experiment in ROI 1

The experiment using the complete dataset (ROI 1) yielded results summarized in Table 2. All evaluated models achieved a high Overall Accuracy of 97%. However, it is important to consider the significant class imbalance in the dataset and examine additional accuracy metrics to gain more informative insights into the models' performance. Notably, U-NET Fusion outperformed the other models in two of the three balanced metrics, particularly in Recall. This suggests its superior ability to correctly identify positive instances and minimize false negatives. On the other hand, U-NET NDVI exhibited the highest Precision but showed relatively weaker performance in the other evaluated metrics. A higher precision value indicates a lower rate of false positive predictions. Although U-NET RGBN Dice Score and Precision slightly underperformed compared to the best model, it still demonstrated notable results. Furthermore, Figure 6 provides examples of successful segmentation, illustrating the models' potential to delineate AR initiatives accurately.

Table 2. Accuracy metrics for the experiment in Region of Interest 1

	Overall Accuracy	Dice Score	Precision	Recall
U-NET RGBN	**0.97**	0.23	0.48	0.25
U-NET NDVI	**0.97**	0.16	**0.52**	0.16
U-NET Fusion	**0.97**	**0.26**	0.51	**0.31**

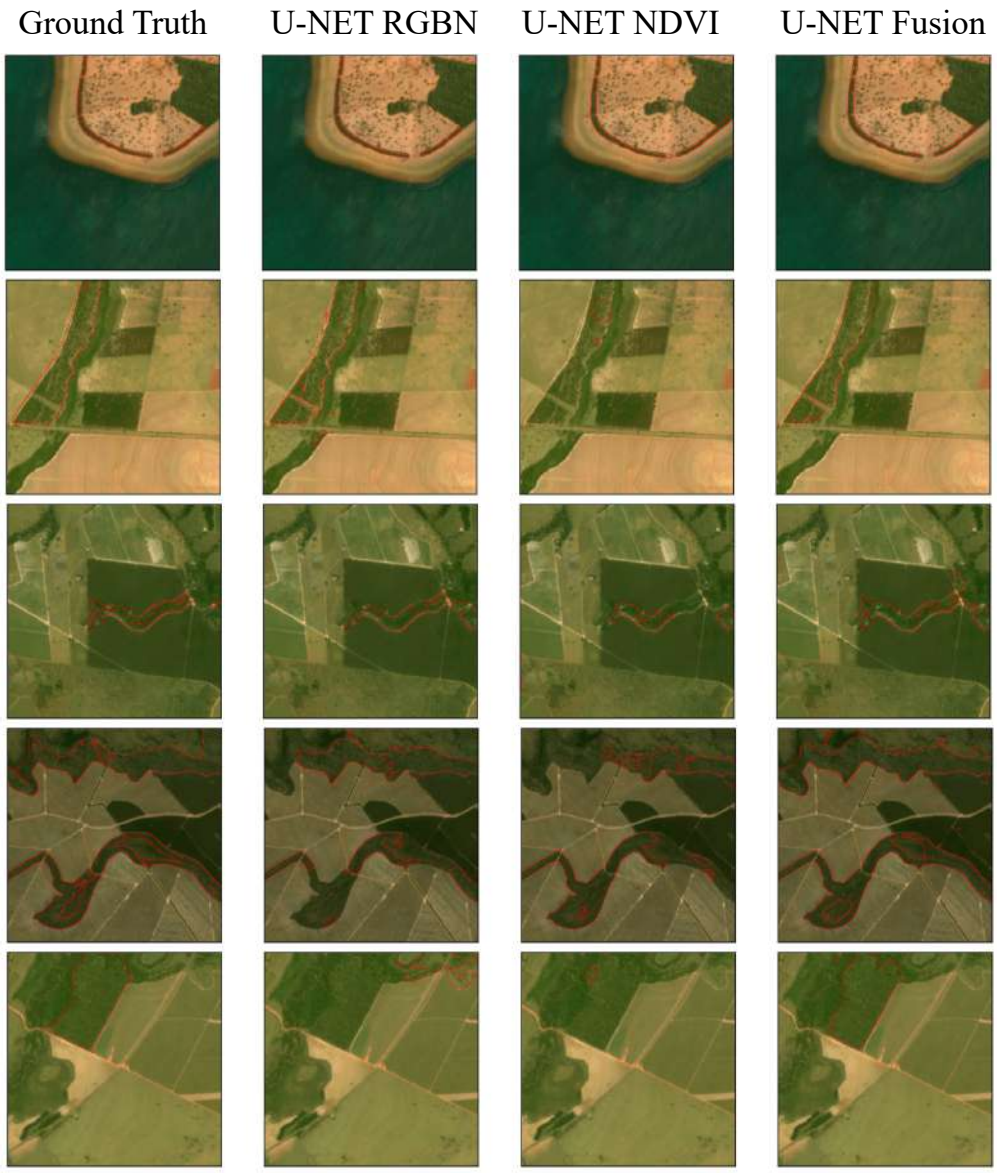

Figure 6: Examples of successful segmentation results in Region of Interest 1, encompassing the entire dataset.

4.2 Experiment in ROI 2

Table 3 presents the results of the second experiment conducted in the reduced dataset (ROI 2). High Overall Accuracy was also observed in all evaluated models (>95%). Nevertheless, the balanced metrics showed considerable improvements compared to the experiment in ROI 1. Specifically, the Dice Score nearly doubled for all models, indicating enhanced spatial alignment. U-NET RGBN showcased superior performance on the reduced dataset, achieving higher balanced accuracy in two out of the three metrics. Similar to the first experiment, U-NET NDVI demonstrated relatively weaker

performance in the evaluated metrics. While U-NET Fusion displayed the best Precision, it showed a slightly weaker performance in the other balanced metrics when compared to U-NET RGBN. Figure 7 provides some examples of successful segmentation for ROI 2.

Table 3. Accuracy metrics for the experiment in Region of Interest 2

	Overall Accuracy	Dice Score	Precision	Recall
U-NET RGBN	**0.96**	**0.40**	0.52	**0.39**
U-NET NDVI	0.95	0.37	0.47	0.38
U-NET Fusion	**0.96**	0.36	**0.54**	0.35

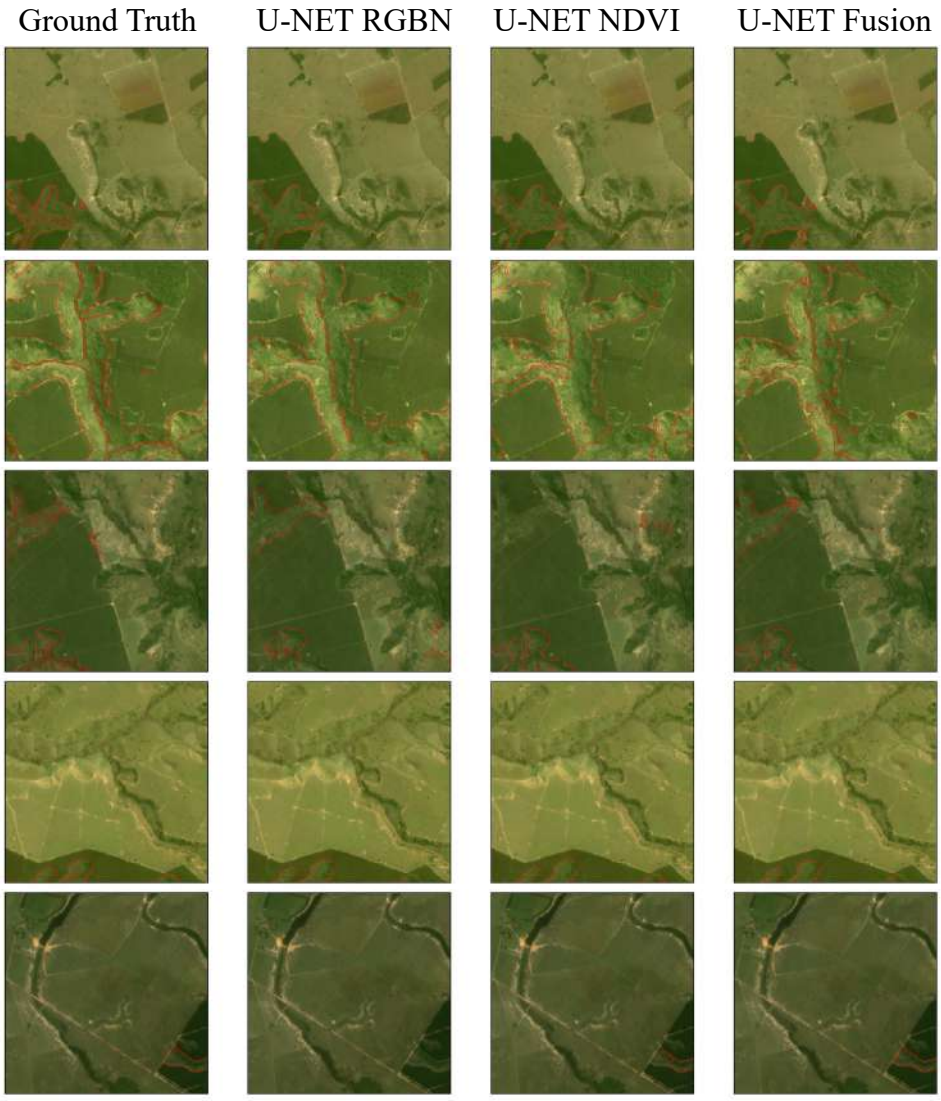

Figure 7: Examples of successful segmentation results in Region of Interest 2, encompassing just a subset of the dataset.

5 Discussion

The findings presented in the previous section indicate that accurately mapping AR initiatives using SRS is a complex task. Although all models achieved high Overall Accuracy, it is important to consider the balanced metrics when analyzing the results due to the prevalence of landscape pixels compared to AR sites. The best results were observed in the experiment conducted in ROI 2, which can be attributed to two potential reasons. Firstly, the relatively homogeneous landscape in ROI 2 facilitates the classifier in creating more accurate representations of the classification target and background. ROI 2 predominantly consists of pasture and silviculture, as depicted in Figure 8. Conversely, ROI 1 encompasses one of the most fragmented landscapes in Brazil [17]. The heterogeneity of tropical landscapes is a well-known challenge in land use and land cover classification tasks [27,28]. Secondly, by reducing the dataset to include only the most informative source of AR polygons, we likely generated a more precise training dataset for calibrating the U-NET model. The accuracy of machine learning models relies heavily on the training set's quality and representativeness, whereas poor-quality inputs cannot produce satisfactory results [29].

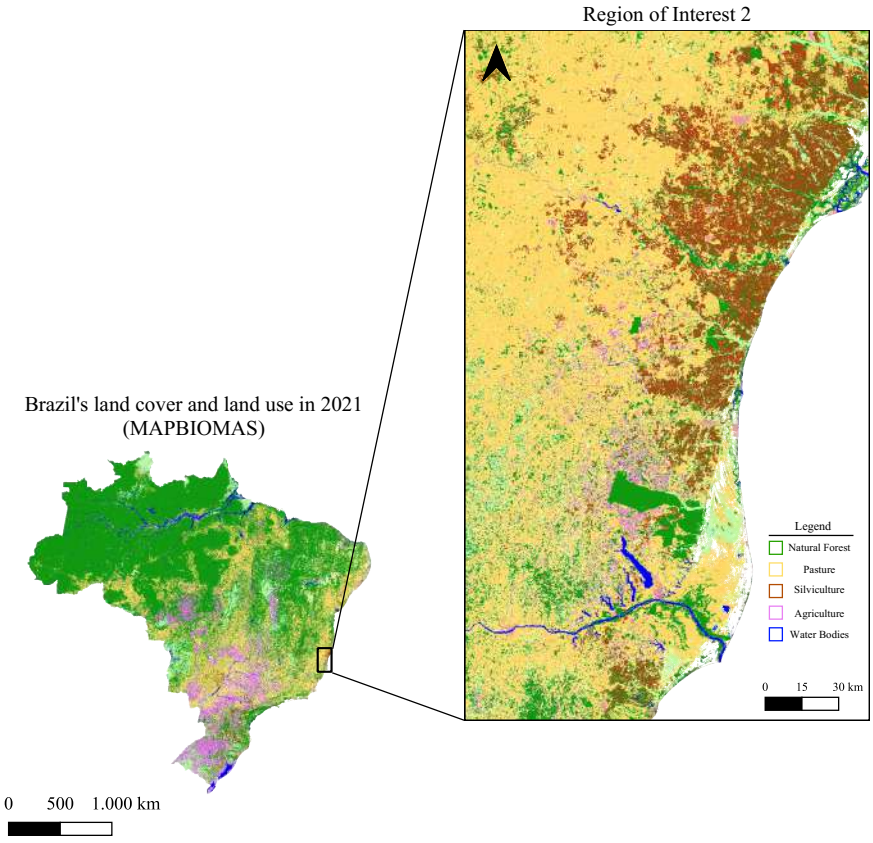

Figure 8: Land cover and land use of ROI 2 in 2021. Source: MAPBIOMAS [17].

Some similar attempts were made before to map Ecological Restoration or regrowing Atlantic Forest. Aguiar [24] classified pixels extracted for AR and PR sites using spectral metrics, temporal spectral metrics, and landscape attributes. That study achieved 87% overall accuracy using a Random Forest model, illustrating that separating those different techniques using SRS imagery is possible. However, Aguiar [24] didn't include elements from the background landscape and worked with a specific hydrographic basin in Brazil. Wagner et al. [30] successfully mapped regrowing Atlantic Forest using ultra-resolution WorldView imagery (0.3-0.5 m), but they didn't analyze if it was derived from natural or human-assisted regrowth. By examining some polygons using high-resolution Google Earth images (>1m), we identified additional features that could significantly enhance the classification of AR initiatives. Consequently, it is worth considering that the spatial resolution offered by Planet Scope data may have presented limitations for the classification task.

Notably, the U-NET NDVI model exhibited the lowest performance among the evaluated models in both experiments. Previous studies, such as Liu et al. [31] and Aguiar [24], have identified the temporal evolution of vegetation indexes as a significant factor in identifying Ecological Restoration sites and classifying AR and PR. A potential explanation for the limited success of the U-NET NDVI model could be attributed to georeferencing errors associated with the Planet Scope data. These errors, reported with an average deviation of less than 10 meters [32], could potentially introduce misalignments of two pixels between each timestamp. Consequently, random variations in NDVI values unrelated to forest growth may emerge, impacting the model's ability to capture the desired information accurately. Other studies have highlighted the challenges posed by spatial misalignment and radiometric inaccuracies of small-satellite constellations in classification tasks, including Planet Scope [33].

The fusion of remote sensing data modalities has proven advantageous in various classification applications [34]. Previous studies have highlighted the benefits of using optical data with different spatial resolutions to map European forest types [35]. In particular, the fusion of RADAR and optical data has emerged as a promising technique in conservation research [36]. The results obtained in the ROI 1 experiment revealed the superiority of the U-NET fusion model over other configurations. Notably, the fusion of SRS layers yielded considerably higher Recall, suggesting that adding additional sensors

can enhance the differentiability between AR sites and the background. In addition, the slight underperformance of the U-NET fusion compared to the U-NET RBGN in ROI 2 can be partially attributed to the region's more homogeneous landscape, requiring less information to perform the segmentation. These findings highlight the potential of utilizing fused SRS modalities, offering valuable insights for classifying AR initiatives. It suggests that by leveraging the complementary information provided by diverse SRS layers, we can enhance the accuracy of mapping and monitoring AR projects in landscapes characterized by varying levels of complexity. Further research can build upon these findings to refine fusion techniques and advance the precise characterization of AR sites across diverse landscapes.

6 Limitations and Future Work

Given the time constraints of this research, we recognize limitations in dataset filtering and hyperparameter tuning. To enhance the performance of the presented models, we suggest the following guidelines for future work:

- Dataset filtering: We suggest using machine learning to filter the dataset more effectively and obtain refined versions. An interesting option would be employing clustering algorithms to isolate a subset of high-quality polygons. Then, calibrate another model, like a Random Forest, using spectral and temporal spectral metrics from the pixels within the polygons to classify the remaining dataset into good and bad quality polygons.

- Hyperparameter tuning: We recommend investing additional time in fine-tuning hyperparameters, such as the learning rate and the number of training epochs. Exploring different loss functions to determine if they yield improved results would also be beneficial. Additionally, considering the size of each image chip as a hyperparameter to tune could be valuable. Decreasing chip size would increase the number of training samples but may reduce landscape information. It would be insightful to conduct tests with various combinations of chip sizes to evaluate their impact on results.

7 Conclusion

To our knowledge, we conducted the first attempt to map an Ecological Restoration method in a large region using high-resolution SRS imagery. Although improvements in accuracy are possible, this study yielded important lessons that will be summarized to address the proposed research questions:

- Q1: To what extent can sites of active forest restoration be mapped using satellite remote sensing imagery?

Our results suggest that SRS imagery show potential for mapping AR, but further improvements are needed to establish a robust methodology for informing environmental policies. Although we compiled an extensive dataset of AR sites, the limitations in metadata and polygon delimitation might influence the calibration of the U-NET models and subsequently affect the results. We recommend implementing additional filtering techniques on the dataset to enhance accuracy metrics.

- Q2: To what extent do temporal remote sensing metrics produce higher classification accuracy than spectral metrics from a single time epoch?

The isolated NDVI temporal metrics yielded no noticeable improvements in classifying AR. Surprisingly, U-NET RGBN outperformed the U-NET NDVI in both experiments. We hypothesize that georeferencing misalignment in the Planet Scope data could introduce spurious signals and diminish its suitability for AR classification.

- Q3: To what extent does fusing different remote sensing modalities increase the accuracy of the predictions?

We observed that fusing different SRS modalities positively influenced the accuracy of classifying AR in heterogeneous landscapes. The U-NET fusion technique exhibited the highest balanced accuracy metrics in ROI 1, known for its mostly fragmented landscape. The high Recall observed in this experiment suggests that the inclusion of different layers assists the model in identifying background features more accurately.

Appendix

A. Code availability

All code is available in the GitHub repository at https://github.com/fnincao/reforestation-CNN/releases/tag/v0.1.0.

B. Acknowledgments

The author extends sincere gratitude to all the advisors and collaborators for their invaluable project guidance and technical support throughout the study:

- Dr. David Commes, Dr. Charlotte Wheeler, and Dr. Srinivasan Keshav from the University of Cambridge

- Dr. Pedro Henrique Santin Brancalion from the School of Agriculture at USP/ESALQ.

- Dr. Paulo Guilherme Molin from the Federal University of São Carlos

- Dr. David Moffat, Dr. James Harding, and Dr. Daniel Clewley from the Plymouth Marine Laboratory

The author would also like to thank the NERC Earth Observation Data Acquisition and Analysis Service (NEODAAS) for access to compute resources for this study. Finally, the author gratefully acknowledges the support and funding provided by the Cambridge Center for Carbon Credits, which greatly contributed to the completion of this study.

C. Remote Sensing of Active Restoration

Satellite Remote Sensing (SRS) is a valuable tool for monitoring ecological restoration initiatives, providing sufficient information to estimate 11 out of the 18 most important forest recovery attributes established by the Society for Ecological Restoration [16]. Additionally, SRS offers unparalleled spatial information and enables more frequent analysis of temporal variations in bio-physical parameters. Notably, temporal metrics were identified as a key factor in the case of differentiating AR from natural regrowth in Taiwanese forests [31]. In contrast to natural regrowth or PR, AR initiatives are mainly characterized by implementing engineering methods for planting native trees [37]. With the expectation that a successful AR site will achieve an initial forest physiognomy of several native trees within less than five years [12], it becomes crucial to employ RS data capable of capturing and analyzing these landscape variations in time. Therefore, the following sections will describe the theoretical basis for the SRS layers utilized in this study:

- Normalized Difference Vegetation Index (NDVI): Passive optical data, such as the Landsat satellite series, provides extensive and enduring SRS imagery. The reflectance of vegetated areas produces a distinct shape in the electromagnetic spectrum, enabling the estimate of a wide range of bio-physical parameters (Figure A1). This data modality has proven highly effective in forestry monitoring, offering valuable insights into critical dynamics like forest growth and deforestation [38]. Due to the limited number of bands in multispectral platforms (i.e., usually blue, green, red, and near-infrared), some spectral indices were developed to enhance vegetation features while mitigating atmospheric effects and illumination-observation geometries [39]. The NDVI was designed to highlight Chlorophyll-*a* spectral feature, a vital protein for plant photosynthesis [22]. In the context of Ecological Restoration monitoring, Chlorophyll-sensitive spectral indices like NDVI are expected to increase as trees grow over time [22]. Additionally, the early stages of forest development exhibit relatively low biomass and percent of canopy cover, resulting in a steady NDVI increase with the forest growth without reaching saturation levels [40].

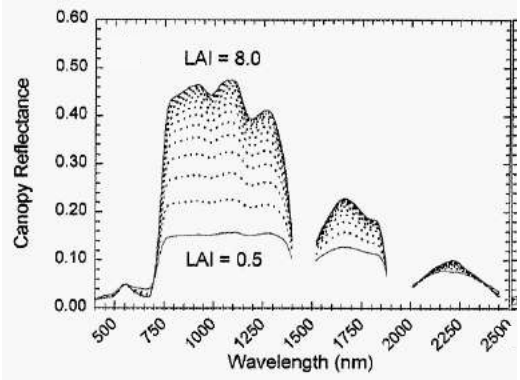

Figure A1: Spectral variation of canopy reflectance with varying Leaf Area Index (LAI). **Adapted from [41].**

- RADAR C-Band and L-Band: With advancements in Synthetic Aperture RADAR (SAR) technology, high spatial resolution RADAR data availability has increased significantly. SAR operates in the microwave region and is an active sensing modality, offering distinct advantages such as reduced sensitivity to atmospheric noise and the ability to image the Earth day and night [42]. One of the most derived products from SAR data is Ground Range Detected (GRD) imagery, which is processed to obtain backscatter coefficients. The backscattering values are proportional to the signal reflected to the sensor and record valuable information about the interactions between electromagnetic energy and the Earth's surface [43]. SAR data has found extensive use in forestry applications due to its superior ability to penetrate forest canopies compared to shorter wavelengths in the optical range [44]. The penetration depth into the forest structure increases as the operating wavelength gets longer (Figure A2). For example, the C-Band SAR (~6 cm) is sensitive to changes in canopy cover and crown properties [43]. On the other hand, the L-Band SAR (~23 cm) exhibits even greater penetration capabilities, offering more precise information about the vertical structure, understory, and biomass [45]. Consequently, as an Ecological Restoration site progresses, C-Band and L-Band backscattering is expected to increase.

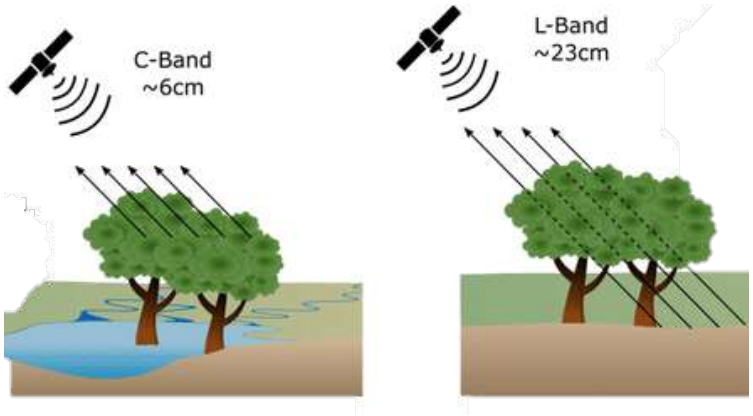

Figure A2. Radar backscattering mechanisms in forested landscapes for different RADAR bands: C-band (left) and L-band (right). **Adapted from [46]**.

D. U-NET for forestry Remote Sensing applications

U-Net is widely regarded as one of the most popular and effective architectures of Fully Convolutional Networks (FCNs) [47]. Unlike traditional neural networks that employ fully connected layers, FCNs rely solely on convolutional layers. A convolutional operation is a dynamic interplay between a sliding window activation filter and an input layer. This process allows the network to extract meaningful features from the input data by convolving the filter across the spatial dimensions [48]. FCNs are often applied to semantic segmentation tasks where each pixel is assigned a class as the final output. Regarding the U-NET architecture [25], it consists of a contracting path, which captures context and reduces spatial dimensions through successive convolutional and pooling layers. The contracting path is followed by an expansion path that leverages upsampling and transposed convolutions to regain spatial resolution and produce the pixel-wise segmentation map. Furthermore, skip connections in U-NET facilitate the integration of high-resolution features from the contracting path to the expanding path, preserving spatial details and enhancing gradient flow (e.g., updating the weights during backpropagation) for improved segmentation accuracy (Figure A3). U-NET's elimination of fully connected layers offers benefits in handling input data of varying resolutions and reduces parameters, enhancing memory efficiency and computational speed [49]. Also, this architecture is recognized for producing accurate outputs with considerably fewer training samples than other Neural Networks frameworks [25].

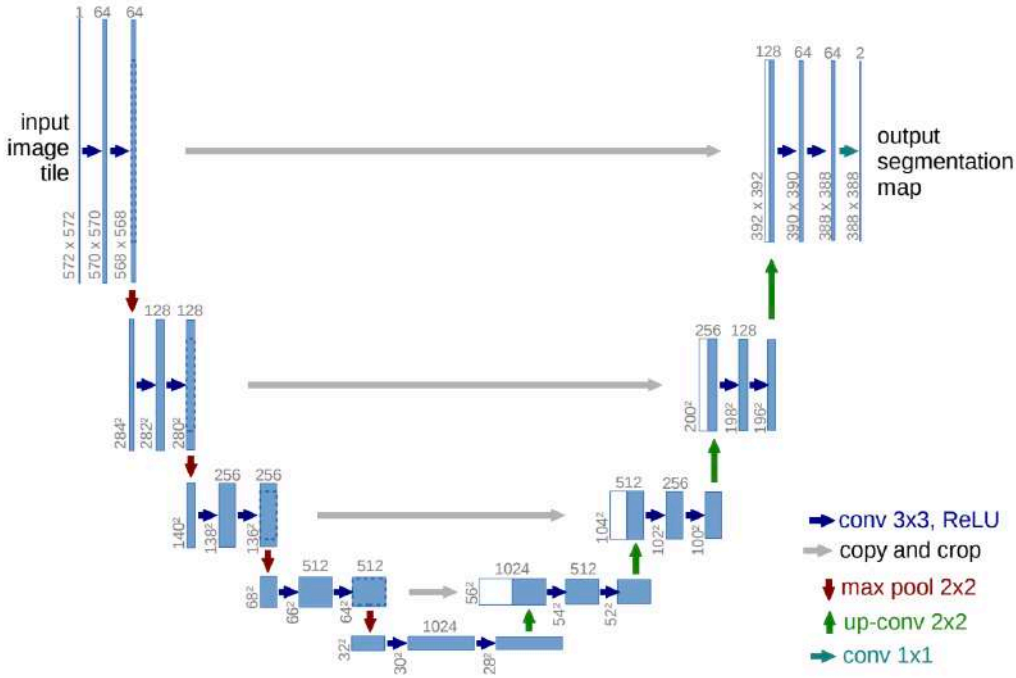

Figure A3. The original U-NET configuration was designed for biological image segmentation. Its name reflects the U-shaped architecture created through the contraction and expansion paths. **Extracted from [25]**

FCNs have been recognized as highly suitable frameworks for forestry remote sensing applications [50]. Given the characteristics of U-NET, this architecture proves to be efficient in processing large volumes of remote sensing images by effectively learning the local and regional contextual spatial information of neighboring pixels [51]. Furthermore, U-NET's flexibility in accommodating various input image sizes makes it adaptable for applications requiring different levels of surrounding information, as well as compatible with all sensor products available. Consequently, several related studies have provided compelling evidence supporting the suitability of U-NET for addressing the objectives of this study. For instance, Zhiyong et al. [52] successfully employed U-NET to predict temporal changes in heterogeneous SRS images, showcasing the architecture's ability to identify patterns using temporal metrics as inputs. U-NET was also utilized to generate automatic deforestation alerts in the Amazon and Atlantic Forest biomes, leveraging a temporal series of Sentinel-2/MSI images [53]. Furthermore, U-NET accurately identified trees across the entire African continent in a large-scale study utilizing high-resolution SRS imagery, demonstrating its scalability capacity [54]. Finally, U-NET was employed in the Atlantic Forest for small-scale (~2410 km2) mapping of degradation, secondary forests, eucalyptus plantation, and the identification of significant tree species using ultra-resolution images [18,30]

References

1. Ribeiro, M.C.; Metzger, J.P.; Martensen, A.C.; Ponzoni, F.J.; Hirota, M.M. The Brazilian Atlantic Forest: How Much Is Left, and How Is the Remaining Forest Distributed? Implications for Conservation. *Biol. Conserv.* **2009**, *142*, 1141–1153, doi:10.1016/j.biocon.2009.02.021.
2. Jenkins, C.N.; Alves, M.A.S.; Uezu, A.; Vale, M.M. Patterns of Vertebrate Diversity and Protection in Brazil. *PLOS ONE* **2015**, *10*, e0145064, doi:10.1371/journal.pone.0145064.
3. Myers, N.; Mittermeier, R.A.; Mittermeier, C.G.; da Fonseca, G.A.B.; Kent, J. Biodiversity Hotspots for Conservation Priorities. *Nature* **2000**, *403*, 853–858, doi:10.1038/35002501.
4. Grelle, C.E.V.; Rajão, H.; Marques, M.C.M. The Future of the Brazilian Atlantic Forest. In *The Atlantic Forest*; Marques, M.C.M., Grelle, C.E.V., Eds.; Springer International Publishing: Cham, 2021; pp. 487–503 ISBN 978-3-030-55321-0.
5. SOS Mata Atlântica; INPE *Atlas dos Remanescentes Florestais da Mata Atlântica*; 2023; p. 61;.
6. UNEP Https://Www.Unep.Org/Interactive/Flagship-Initiatives-Boosting-Nature-Livelihoods/ Available online: https://www.unep.org/interactive/flagship-initiatives-boosting-nature-livelihoods/ (accessed on 17 June 2023).
7. Clewell, A.; Aronson, J.; Winterhalder, K. Society for Ecological Restoration International Science & Policy Working Group. *SER Int. Primer Ecol. Restor.* **2004**.
8. Shono, K.; Cadaweng, E.A.; Durst, P.B. Application of Assisted Natural Regeneration to Restore Degraded Tropical Forestlands. *Restor. Ecol.* **2007**, *15*, 620–626, doi:10.1111/j.1526-100X.2007.00274.x.
9. Holl, K.D.; Aide, T.M. When and Where to Actively Restore Ecosystems? *For. Ecol. Manag.* **2011**, *261*, 1558–1563, doi:10.1016/j.foreco.2010.07.004.
10. Chazdon, R.L.; Guariguata, M.R. Natural Regeneration as a Tool for Large-scale Forest Restoration in the Tropics: Prospects and Challenges. *Biotropica* **2016**, *48*, 716–730, doi:10.1111/btp.12381.
11. Meli, P.; Holl, K.D.; Rey Benayas, J.M.; Jones, H.P.; Jones, P.C.; Montoya, D.; Moreno Mateos, D. A Global Review of Past Land Use, Climate, and Active vs. Passive Restoration Effects on Forest Recovery. *PLOS ONE* **2017**, *12*, e0171368, doi:10.1371/journal.pone.0171368.
12. Brancalion, P.H.S.; Schweizer, D.; Gaudare, U.; Mangueira, J.R.; Lamonato, F.; Farah, F.T.; Nave, A.G.; Rodrigues, R.R. Balancing Economic Costs and Ecological Outcomes of Passive and Active Restoration in Agricultural Landscapes: The Case of Brazil. *Biotropica* **2016**, *48*, 856–867, doi:10.1111/btp.12383.
13. Heinrich, V.H.A.; Dalagnol, R.; Cassol, H.L.G.; Rosan, T.M.; De Almeida, C.T.; Silva Junior, C.H.L.; Campanharo, W.A.; House, J.I.; Sitch, S.; Hales, T.C.; et al. Large Carbon Sink Potential of Secondary Forests in the Brazilian Amazon to Mitigate Climate Change. *Nat. Commun.* **2021**, *12*, 1785, doi:10.1038/s41467-021-22050-1.
14. Rodrigues, R.R.; Gandolfi, S.; Nave, A.G.; Aronson, J.; Barreto, T.E.; Vidal, C.Y.; Brancalion, P.H.S. Large-Scale Ecological Restoration of High-Diversity Tropical Forests in SE Brazil. *For. Ecol. Manag.* **2011**, *261*, 1605–1613, doi:10.1016/j.foreco.2010.07.005.
15. Crouzeilles, R.; Santiami, E.; Rosa, M.; Pugliese, L.; Brancalion, P.H.S.; Rodrigues, R.R.; Metzger, J.P.; Calmon, M.; Scaramuzza, C.A.D.M.; Matsumoto, M.H.; et al. There Is Hope for Achieving Ambitious Atlantic Forest Restoration

Commitments. *Perspect. Ecol. Conserv.* **2019**, *17*, 80–83, doi:10.1016/j.pecon.2019.04.003.
16. McKenna, P.B.; Lechner, A.M.; Hernandez Santin, L.; Phinn, S.; Erskine, P.D. Measuring and Monitoring Restored Ecosystems: Can Remote Sensing Be Applied to the Ecological Recovery Wheel to Inform Restoration Success? *Restor. Ecol.* **2023**, *31*, doi:10.1111/rec.13724.
17. Souza, C.M.; Z. Shimbo, J.; Rosa, M.R.; Parente, L.L.; A. Alencar, A.; Rudorff, B.F.T.; Hasenack, H.; Matsumoto, M.; G. Ferreira, L.; Souza-Filho, P.W.M.; et al. Reconstructing Three Decades of Land Use and Land Cover Changes in Brazilian Biomes with Landsat Archive and Earth Engine. *Remote Sens.* **2020**, *12*, 2735, doi:10.3390/rs12172735.
18. Wagner, F.H.; Sanchez, A.; Tarabalka, Y.; Lotte, R.G.; Ferreira, M.P.; Aidar, M.P.M.; Gloor, E.; Phillips, O.L.; Aragão, L.E.O.C. Using the U-net Convolutional Network to Map Forest Types and Disturbance in the Atlantic Rainforest with Very High Resolution Images. *Remote Sens. Ecol. Conserv.* **2019**, *5*, 360–375, doi:10.1002/rse2.111.
19. Assunção, J.; Almeida, C.; Gandour, C. Brazil Needs to Monitor Its Tropical Regeneration: Remote Monitoring System Is Technologically Feasible, but Needs Public Policy Support. *Clim. Policy Initiat.* **2020**.
20. Duarte, L.D.S.; Bergamin, R.S.; Marcilio-Silva, V.; Seger, G.D.D.S.; Marques, M.C.M. Phylobetadiversity among Forest Types in the Brazilian Atlantic Forest Complex. *PLoS ONE* **2014**, *9*, e105043, doi:10.1371/journal.pone.0105043.
21. Cantidio, L.S.; Souza, A.F. Aridity, Soil and Biome Stability Influence Plant Ecoregions in the Atlantic Forest, a Biodiversity Hotspot in South America. *Ecography* **2019**, *42*, 1887–1898, doi:10.1111/ecog.04564.
22. Huang, S.; Tang, L.; Hupy, J.P.; Wang, Y.; Shao, G. A Commentary Review on the Use of Normalized Difference Vegetation Index (NDVI) in the Era of Popular Remote Sensing. *J. For. Res.* **2021**, *32*, 1–6, doi:10.1007/s11676-020-01155-1.
23. Trenčanová, B.; Proença, V.; Bernardino, A. Development of Semantic Maps of Vegetation Cover from UAV Images to Support Planning and Management in Fine-Grained Fire-Prone Landscapes. *Remote Sens.* **2022**, *14*, 1262, doi:10.3390/rs14051262.
24. Aguiar, N.V.V. Uso do histórico, presente e contexto da paisagem na discriminação de florestas jovens em restauração ativa e regeneração natural. Mestrado em Recursos Florestais, Universidade de São Paulo: Piracicaba, 2022.
25. Ronneberger, O.; Fischer, P.; Brox, T. U-Net: Convolutional Networks for Biomedical Image Segmentation. In *Medical Image Computing and Computer-Assisted Intervention – MICCAI 2015*; Navab, N., Hornegger, J., Wells, W.M., Frangi, A.F., Eds.; Lecture Notes in Computer Science; Springer International Publishing: Cham, 2015; Vol. 9351, pp. 234–241 ISBN 978-3-319-24573-7.
26. Li, X.; Sun, X.; Meng, Y.; Liang, J.; Wu, F.; Li, J. Dice Loss for Data-Imbalanced NLP Tasks 2020.
27. Hurskainen, P.; Adhikari, H.; Siljander, M.; Pellikka, P.K.E.; Hemp, A. Auxiliary Datasets Improve Accuracy of Object-Based Land Use/Land Cover Classification in Heterogeneous Savanna Landscapes. *Remote Sens. Environ.* **2019**, *233*, 111354, doi:10.1016/j.rse.2019.111354.
28. Mishra, V.N.; Prasad, R.; Rai, P.K.; Vishwakarma, A.K.; Arora, A. Performance Evaluation of Textural Features in Improving Land Use/Land Cover Classification Accuracy of Heterogeneous Landscape Using Multi-Sensor Remote Sensing Data. *Earth Sci. Inform.* **2019**, *12*, 71–86, doi:10.1007/s12145-018-0369-z.
29. Jain, A.; Patel, H.; Nagalapatti, L.; Gupta, N.; Mehta, S.; Guttula, S.; Mujumdar,

S.; Afzal, S.; Sharma Mittal, R.; Munigala, V. Overview and Importance of Data Quality for Machine Learning Tasks. In Proceedings of the Proceedings of the 26th ACM SIGKDD International Conference on Knowledge Discovery & Data Mining; ACM: Virtual Event CA USA, August 23 2020; pp. 3561–3562.
30. Wagner, F.H.; Sanchez, A.; Aidar, M.P.M.; Rochelle, A.L.C.; Tarabalka, Y.; Fonseca, M.G.; Phillips, O.L.; Gloor, E.; Aragão, L.E.O.C. Mapping Atlantic Rainforest Degradation and Regeneration History with Indicator Species Using Convolutional Network. *PLOS ONE* **2020**, *15*, e0229448, doi:10.1371/journal.pone.0229448.
31. Liu, C.-C.; Chen, Y.-H.; Wu, M.-H.M.; Wei, C.; Ko, M.-H. Assessment of Forest Restoration with Multitemporal Remote Sensing Imagery. *Sci. Rep.* **2019**, *9*, 7279, doi:10.1038/s41598-019-43544-5.
32. Ghuffar, S. DEM Generation from Multi Satellite PlanetScope Imagery. *Remote Sens.* **2018**, *10*, 1462, doi:10.3390/rs10091462.
33. Leach, N.; Coops, N.C.; Obrknezev, N. Normalization Method for Multi-Sensor High Spatial and Temporal Resolution Satellite Imagery with Radiometric Inconsistencies. *Comput. Electron. Agric.* **2019**, *164*, 104893, doi:10.1016/j.compag.2019.104893.
34. Li, J.; Hong, D.; Gao, L.; Yao, J.; Zheng, K.; Zhang, B.; Chanussot, J. Deep Learning in Multimodal Remote Sensing Data Fusion: A Comprehensive Review. *Int. J. Appl. Earth Obs. Geoinformation* **2022**, *112*, 102926, doi:10.1016/j.jag.2022.102926.
35. Kempeneers, P.; Sedano, F.; Seebach, L.; Strobl, P.; San-Miguel-Ayanz, J. Data Fusion of Different Spatial Resolution Remote Sensing Images Applied to Forest-Type Mapping. *IEEE Trans. Geosci. Remote Sens.* **2011**, *49*, 4977–4986, doi:10.1109/TGRS.2011.2158548.
36. Schulte To Bühne, H.; Pettorelli, N. Better Together: Integrating and Fusing Multispectral and Radar Satellite Imagery to Inform Biodiversity Monitoring, Ecological Research and Conservation Science. *Methods Ecol. Evol.* **2018**, *9*, 849–865, doi:10.1111/2041-210X.12942.
37. Brancalion, P.H.S.; Holl, K.D. Guidance for Successful Tree Planting Initiatives. *J. Appl. Ecol.* **2020**, *57*, 2349–2361, doi:10.1111/1365-2664.13725.
38. Banskota, A.; Kayastha, N.; Falkowski, M.J.; Wulder, M.A.; Froese, R.E.; White, J.C. Forest Monitoring Using Landsat Time Series Data: A Review. *Can. J. Remote Sens.* **2014**, *40*, 362–384, doi:10.1080/07038992.2014.987376.
39. Montero, D.; Aybar, C.; Mahecha, M.D.; Martinuzzi, F.; Söchting, M.; Wieneke, S. A Standardized Catalogue of Spectral Indices to Advance the Use of Remote Sensing in Earth System Research. *Sci. Data* **2023**, *10*, 197, doi:10.1038/s41597-023-02096-0.
40. Verly, O.M.; Vieira Leite, R.; Da Silva Tavares-Junior, I.; José Silva Soares Da Rocha, S.; Garcia Leite, H.; Marinaldo Gleriani, J.; Paula Miranda Xavier Rufino, M.; De Fatima Silva, V.; Moreira Miquelino Eleto Torres, C.; Plata-Rueda, A.; et al. Atlantic Forest Woody Carbon Stock Estimation for Different Successional Stages Using Sentinel-2 Data. *Ecol. Indic.* **2023**, *146*, 109870, doi:10.1016/j.ecolind.2023.109870.
41. NV5 Canopies Available online: https://www.l3harrisgeospatial.com/docs/Canopies.html (accessed on 18 June 2023).
42. Tsokas, A.; Rysz, M.; Pardalos, P.M.; Dipple, K. SAR Data Applications in Earth Observation: An Overview. *Expert Syst. Appl.* **2022**, *205*, 117342, doi:10.1016/j.eswa.2022.117342.
43. Flores-Anderson, A.I.; Herndon, K.E.; Thapa, R.B.; Cherrington, E. *The SAR Handbook: Comprehensive Methodologies for Forest Monitoring and Biomass Estimation*; 2019;

44. Papathanassiou, K.P.; Cloude, S.R.; Pardini, M.; Quiñones, M.J.; Hoekman, D.; Ferro-Famil, L.; Goodenough, D.; Chen, H.; Tebaldini, S.; Neumann, M.; et al. Forest Applications. In *Polarimetric Synthetic Aperture Radar*; Hajnsek, I., Desnos, Y.-L., Eds.; Remote Sensing and Digital Image Processing; Springer International Publishing: Cham, 2021; Vol. 25, pp. 59–117 ISBN 978-3-030-56502-2.
45. Le Toan, T.; Beaudoin, A.; Riom, J.; Guyon, D. Relating Forest Biomass to SAR Data. *IEEE Trans. Geosci. Remote Sens.* **1992**, *30*, 403–411, doi:10.1109/36.134089.
46. Ottinger, M.; Kuenzer, C. Spaceborne L-Band Synthetic Aperture Radar Data for Geoscientific Analyses in Coastal Land Applications: A Review. *Remote Sens.* **2020**, *12*, 2228, doi:10.3390/rs12142228.
47. Siddique, N.; Paheding, S.; Elkin, C.P.; Devabhaktuni, V. U-Net and Its Variants for Medical Image Segmentation: A Review of Theory and Applications. *IEEE Access* **2021**, *9*, 82031–82057, doi:10.1109/ACCESS.2021.3086020.
48. Dumoulin, V.; Visin, F. A Guide to Convolution Arithmetic for Deep Learning. **2016**, doi:10.48550/ARXIV.1603.07285.
49. Françani, A.O. Analysis of the Performance of U-Net Neural Networks for the Segmentation of Living Cells. **2022**, doi:10.48550/ARXIV.2210.01538.
50. Kattenborn, T.; Leitloff, J.; Schiefer, F.; Hinz, S. Review on Convolutional Neural Networks (CNN) in Vegetation Remote Sensing. *ISPRS J. Photogramm. Remote Sens.* **2021**, *173*, 24–49, doi:10.1016/j.isprsjprs.2020.12.010.
51. Wang, X.; Hu, Z.; Shi, S.; Hou, M.; Xu, L.; Zhang, X. A Deep Learning Method for Optimizing Semantic Segmentation Accuracy of Remote Sensing Images Based on Improved UNet. *Sci. Rep.* **2023**, *13*, 7600, doi:10.1038/s41598-023-34379-2.
52. Lv, Z.; Huang, H.; Gao, L.; Benediktsson, J.A.; Zhao, M.; Shi, C. Simple Multiscale UNet for Change Detection With Heterogeneous Remote Sensing Images. *IEEE Geosci. Remote Sens. Lett.* **2022**, *19*, 1–5, doi:10.1109/LGRS.2022.3173300.
53. Bragagnolo, L.; Da Silva, R.V.; Grzybowski, J.M.V. Towards the Automatic Monitoring of Deforestation in Brazilian Rainforest. *Ecol. Inform.* **2021**, *66*, 101454, doi:10.1016/j.ecoinf.2021.101454.
54. Reiner, F.; Brandt, M.; Tong, X.; Skole, D.; Kariryaa, A.; Ciais, P.; Davies, A.; Hiernaux, P.; Chave, J.; Mugabowindekwe, M.; et al. More than One Quarter of Africa's Tree Cover Is Found Outside Areas Previously Classified as Forest. *Nat. Commun.* **2023**, *14*, 2258, doi:10.1038/s41467-023-37880-4.